Journal of Bone and Mineral Research, 2025, **00**, 1–10
https://doi.org/10.1093/jbmr/zjaf088
Advance access publication: June 24, 2025
Research Article

Infigratinib low dose therapy is an effective strategy to treat hypochondroplasia

Benoit Demuynck[1], Bhavik P. Shah[2], Franck Mayeux[1], Laurine Vasseur[3], Florent Barbault[3], Jixin Ding[2], Morgan Paull[2], Tejaswini Reddi[2], Elena Muslimova[2], Laurence Legeai-Mallet[1,*]

[1]Imagine Institute, INSERM UMR 1163, Université de Paris Cité, F-75015 Paris, France
[2]BridgeBio Pharma, QEd Therapeutics, San Francisco, 94158 CA, United States
[3]CNRS, ITODYS, Université Paris Cité, F-75013 Paris, France

*Corresponding author: Laurence Legeai-Mallet, Imagine Institute, INSERM UMR 1163, Université de Paris Cité, 24 boulevard du Montparnasse F-75015 Paris, France (Laurence.legeai-mallet@inserm.fr).

Abstract

Hypochondroplasia is a rare genetic form of skeletal dysplasia, caused by gain-of-function pathogenic variants in the FGF receptor 3 (FGFR3). It is characterized by disproportionate short stature and has a wide spectrum of clinical features. Currently, there are no precision therapeutic options approved for hypochondroplasia. Infigratinib is an orally bioavailable FGFR1-3 selective tyrosine kinase inhibitor in development for achondroplasia and hypochondroplasia. Infigratinib acts directly at the source of the pathophysiological cause of both conditions by inhibiting the phosphorylation of FGFR3 and attenuating both main downstream signaling pathways that are involved in the conditions. Results from a phase 2 study support the concept that infigratinib has a potential to improve bone growth in achondroplasia. We report results of a step-wise evaluation of the therapeutic relevance of infigratinib for hypochondroplasia: in silico assessment of infigratinib with hypochondroplasia associated FGFR3 variants suggest strong interaction; in vitro, infigratinib showed potent inhibitory effect; in a mouse model of hypochondroplasia (*Fgfr3*$^{N534K/+}$), infigratinib resulted in significant improvement in skeletal growth. These data in addition to the clinical results from the phase 2 study conducted in children with achondroplasia provide support for the development of infigratinib in the treatment of hypochondroplasia.

Keywords: FGF receptor 3, hypochondroplasia, achondroplasia, infigratinib, skeletal dysplasia

Lay Summary

Hypochondroplasia is a rare skeletal dysplasia, caused by gain-of-function variants in the FGF receptor 3 (FGFR3). Currently, there are no precision therapeutic options approved for hypochondroplasia. Recent phase 2 trial data of infigratinib in achondroplasia supports the concept that infigratinib has potential to improve bone growth in FGFR-related skeletal dysplasias. Here, we report results of the evaluation of the therapeutic relevance of infigratinib for hypochondroplasia. Infigratinib showed potent inhibitory effect in cellular model and significantly improved skeletal growth in a mouse model of hypochondroplasia. These data provide support for the development of infigratinib in the treatment of hypochondroplasia.

Introduction

Hypochondroplasia (HCH) is a rare form of skeletal dysplasia with an estimated prevalence of approximately 1:15 000 to 1:40 000.[1,2] It is characterized by disproportionate short stature and has a wide spectrum of phenotypes and clinical features.[1] Medical challenges vary greatly between individuals and might include otitis media, language and speech developmental delay, neurocognitive difficulties,[3] and epilepsy;[4,5] however, some individuals may not experience any medical challenges beyond short stature. Quality of life (QoL) data in individuals with HCH is limited. It has been reported that children with HCH tend to exhibit diminished QoL scores, as indicated by parental reports, particularly in the areas of physical and social well-being.[6] Children with HCH are usually diagnosed in early childhood (approximately ages 2-5 yr)[1] and some even later in life when the disproportion becomes more prominent.[7,8] Similar to achondroplasia (ACH), the most common short-limbed skeletal dysplasia, HCH is caused by autosomal dominant gain-of-function mutations in the FGF receptor 3 (*FGFR3*) gene.[9,10] FGF receptor 3, a receptor tyrosine kinase, is a key regulator of bone growth through inhibiting chondrocytes' proliferation and differentiation.[11] Achondroplasia is primarily driven by a G380R-encoding gain-of-function mutation[12] localized in the transmembrane domain of FGFR3. In contrast, there is greater heterogeneity in the *FGFR3* mutations associated with HCH, which is driven by other gain-of-function mutations, most notably the substitution of asparagine for lysine at amino acid position 540 (ie, *FGFR3* N540K) localized in the tyrosine kinase domain.[1,13] Various studies show that the HCH-associated mutation leads to increased phosphorylation of the receptor and activation of downstream signaling.[14] There are currently

Received: March 20, 2025. **Revised:** May 28, 2025. **Accepted:** June 5, 2025

no approved therapeutic options for HCH and management of the condition is currently focused on treating specific complications.[1]

In a phase 2 clinical trial in children with ACH, treatment with infigratinib, an orally bioavailable FGFR1-3 selective tyrosine kinase inhibitor (TKI), resulted in a sustained increase in annualized height velocity (AHV) up to 18 mo (last measured timepoint) and a decrease in upper-to-lower body segment ratio.[15] Using a therapeutic approach for HCH similar to ACH is scientifically plausible due to the similarities in pathophysiology between the 2 conditions. In this study, we hypothesized that infigratinib (BGJ398) could improve defective endochondral and membranous ossification, thus ameliorating the HCH phenotype in the *Fgfr3*$^{N534K/+}$ mouse model of HCH. To provide proof of concept that infigratinib is a relevant therapeutic approach for HCH, we conducted and combined in silico, in vitro, and in vivo studies. First, in silico modeling has shown that infigratinib fits in the ATP-binding pocket of the FGFR3 receptor, and that the N540K mutation creates a loop in one portion of the protein, furthering the interaction between infigratinib and the FGFR3 protein. These results together demonstrate that infigratinib interacts with both the WT and mutated FGFR3 complexes, with a stronger interaction observed in the presence of the N540K pathogenic variant. Second, in vitro studies have demonstrated that infigratinib has single digit-nanomolar potency against 9 different pathogenic variants associated with HCH, including N540K, N540S, N540T, K650Q, K650N, K650T, R223C, T264M, and S351F, and is similar to the potency of the ACH-associated FGFR3 variant (G380R). These data suggest that infigratinib has the potential to counteract the underlying FGFR3 overactivity in HCH as in ACH. Finally, we performed in vivo studies using a mouse model that mimics the human HCH phenotype (*Fgfr3*$^{N534K/+}$) to investigate the effect of infigratinib during bone development.[14] Administration of infigratinib (1 mg/kg/d) s.c. on postnatal days$^{3-24}$ inhibited the constitutive activation of FGFR3 and improved both appendicular and axial skeletal bone growth. In summary, these results provide the first preclinical proof of concept for infigratinib in HCH, validating its therapeutic rationale in this condition.

Materials and methods

Computational methodology

All computations were performed on the FGFR3 tyrosine kinase domain, WT and N540K (HCH variant), using the PDB structure (7DHL).[16] The initial position of infigratinib in the catalytic site was determined based on prior investigation.[17,18] Molecular dynamics (MD) simulations were engaged for the FGFR3-WT and FGFR3-N540K kinase structures with and without infigratinib using the AMBER[19] software for 500 ns within water boxes. All simulations were replicated 3 times and structural analyses were performed with VMD[20] and CPPTRAJ[21] software. The umbrella sampling (US) technique[22] was used to determine the free energy for the non-covalent association of infigratinib with FGFR3-WT and FGFR3-N540K using the distance between the ligand and the catalytic site as variable. The potential of mean force (PMF) curves were then calculated using the WHAM.[23] Further details may be found in the supplementary information section.

In vitro potency of infigratinib

The in vitro potency of infigratinib and its metabolites was assessed against 9 pathogenic *FGFR3* variants associated with HCH (N540K, N540S, N540T, K650Q, K650N, K650T, R223C, T264M, S351F; Invitae Corporation, San Francisco, CA, USA) and compared with the ACH-associated G380R *FGFR3* variant. Stable cells lines were generated for each variant in ATDC5 cells, a mouse chondrogenic cell line.[24] Nine pathogenic *FGFR3* (NM_000142) variants associated with HCH (N540K, N540S, N540T, K650Q, K650N, K650T, R223C, T264M, S351F; Invitae Corporation, San Francisco, CA, USA) were introduced by 2-step PCR and cloned into BamHI/NheI sites of pLVpuro-EF1a-FGFR3c vector. All FGFR3c variants were confirmed by Sanger sequencing. The point mutations of FGFR3c-HCH Lentivirus were produced in 293T cells and transduced into chondrogenic cell line ATDC5 and selected with 2 μg/mL puromycin for 2 wk, maintained in 1 μg/mL puromycin conditions medium. ATDC5-FGFR3-IIIc-HCHs cells and G380R cells were maintained in DMEM: Ham's F12 (1:1) + 2 mM Glutamine +5% FBS and 1 μg/mL puromycin. The expression of FGFR3 protein was confirmed by western blot analysis. In vitro potency evaluated using the phosphorylated ERK (pERK)/ERK ELISA (Cell Signaling Technology, Danvers, MA 01923, USA). Cell lines were incubated with infigratinib under serum-free conditions, then stimulated with FGF2. Levels of pERK1/2 and total ERK1/2 in cell lysates were quantified using ELISA by manufacture described. Median IC50 values for infigratinib and its metabolites against pERK were determined in 3 or more independent experiments and the mean was calculated; each biological replicate comprised 2 technical replicates. Each experiment also included the G380R ACH variant as a positive control.

Mouse model and infigratinib treatment

The *Fgfr3*$^{N534K/+}$ mouse model was generated by crossing CMV-Cre mice (C57BL/6 J) with mice exhibiting germline transmission of the *N534K* mutation corresponding to the human *N540K* (HCH) *FGFR3* mutation.[14] Mice were genotyped using PCRs of total DNA extracted from a sample of external ear tissue. Animal procedures were approved by the French Ministry of Research and the Animal Care and Use Committee at Université Paris Cité (APAFIS#24826-2018080216094268 v5) and were conducted in compliance with ethical principles at the LEAT Facility (Imagine Institute, Paris, France).

Infigratinib was administrated s.c. to *Fgfr3*$^{N534K/+}$ mice during their growth phase. Infigratinib phosphate, the phosphate salt of infigratinib, was formulated as a suspension in HCl 3.5 mM, DMSO 5% for s.c. administration, rather than oral gavage, because of the size of the mice. Mice were treated using 2 dose regiments: either with infigratinib 1 mg/kg s.c. every 3 d from P3 to P15 (birth = day 0) then sacrificed on day 18 (intermittent dosing), or with infigratinib 1 mg/kg s.c. once daily from P3 to P23 then sacrificed on day 24 (daily dosing). Details of treatment groups are shown in Table 1. Clinical observations of potential treatment side effects were performed every 3 d (hind-limb movement, posture, tail, paws). Detailed clinical observations were made at the time of scoring. Naso-anal and tail length measurements were made every 3 d using a ruler. At necroscopy, bone, naso-anal, and

tail lengths were measured using a caliper (VWRi819-0013, VWR International, USA).

In all analyses, WT (*Fgfr3*$^{+/+}$) littermates were used as controls. Both males and females were used in experiments because no significant sex differences have been observed for the biological processes studied herein.

Microradiography and CT images

Lateral and face X-ray images were taken using the Faxitron MX20 Cabinet X-ray system (Lincolnshire, IL, USA) following terminal sacrifice.

Micro-CT imaging of the skull was performed with a Skyscan 1172 system (Bruker MicroCT NV, Kontich, Belgium). For morphological analyses, the skull of mutants and controls were fixed in 70% ethanol. The scan settings were as follows: 80 kV, 100 μA, a pixel resolution of 19.98 μm, rotation steps of 0.5°, and a 0.5 mm aluminum filter. Three-dimensional reconstructions were generated using Avizo software (ThermoFisher Scientific, Waltham, MA, USA).

Histology and immunohistochemistry

All samples were collected in 4% paraformaldehyde, fully decalcified in 0.8 M EDTA (pH 8.0) and embedded in paraffin. Six μm serial sections were prepared. All slices were deparaffinized in Neo-clear solution (Merck Millipore, Darmstadt, Germany) and then rehydrated prior to standard immunostaining. Sections were stained with H&E using standard protocols. Right femur and lumbar vertebra segments L4-L6 were fixed in 4% paraformaldehyde, decalcified with EDTA 0.5 M and embedded in paraffin. Selected adjacent slides were stained using standard immunohistochemical protocols[14] and antibodies against collagen type X (Col X) (1:100, 1-CO097-05, Quartett, Berlin, Germany), collagen type I (1:1000, 20 151-1, Novotec, Lyon, France), and phosphorylated ERK1/2 (1:1000, # 4370S, Cell Signaling, Danvers, MA, USA) using the Dako Envision kit (Dako North America, Inc, Carpinteria, CA, USA). Images were captured with an Olympus PD70-IX2- UCB microscope and CellSens software (Olympus, Tokyo, Japan).

Statistical analysis

Differences between experimental groups were assessed using the Mann-Whitney *U* test. The significance threshold was set at $p < .05$. Statistical analyses were performed using GraphPad PRISM (version 8.4.2; GraphPad Software, San Diego, CA, USA). All values are shown as mean ± SD.

Study design

Animal procedures were approved by the French Ministry of Research and the Animal Care and Use Committee at Université Paris Cité (APAFIS#24826-2018080216094268 v5) and were conducted in compliance with ethical principles at the LEAT Facility (Imagine Institute, Paris, France).

Results

In silico analyses of the interaction of infigratinib with HCH variant

Calculations performed using the US technique enabled the determination of the binding free energy. It was found that the FGFR3-N540K mutant exhibits a significantly lower binding free energy compared to the WT FGFR3-WT (−10.9 kcal/mol vs −6.3 kcal/mol, respectively). These findings indicate that the N540K mutation enhances the inhibitory interaction with infigratinib, likely by promoting a more favorable binding conformation through the loop570-590. During the MD simulations, infigratinib was observed to persist within the active site of either FGFR3-WT or FGFR3-N540K, which is consistent with its role as an inhibitor. It is noteworthy that the N540K amino acid is located on the opposite face of the kinase active site, at a distance of approximately 8.5 Å. As a result, the mutation exerts an indirect and subtle effect. A novel behavior was identified in a loop spanning residues 570 to 590 within the C-terminal domain of the kinase. This loop (referred to L570-90) was observed to move in closer proximity to the kinase active site and form a supplementary favorable electrostatic interaction of D580 with infigratinib in FGFR3-N540K but not in FGFR3-WT (Figure 1). This specific behavior of L570-90 was also observed in the free protein states, though to a lesser extent, which suggests that infigratinib plays a role in an induced fit inhibition. To corroborate these observations, the free energy of interaction between infigratinib and FGFR3-WT or FGFR3-N540K was accurately calculated using US.

The free energy of interaction was determined to be −6.2 kcal/mol for FGFR3-WT and −10.9 kcal/mol for FGFR3-N540K, thereby demonstrating that the approach of L570-90 enables significantly stronger inhibition of infigratinib in the mutant than in the WT. A comprehensive structural examination revealed that the mutation induces a complex network of electrostatic interactions involving charged amino acids, which reorganizes the altered structure. This reorganization facilitates the movement of toward the active site, thus promoting improved binding of infigratinib. It is notable that, to the best of our knowledge, this represents the first observation of inhibition involving this kinase loop.[25,26] This originality confers selectivity, as the L570-90 loop is absent in many kinases[27] and belongs to one of the rare regions without a specific name[28] due to its distance from the active site. In the case of FGFR3, the N540K pathogenic variant, associated with HCH, facilitates this inhibition through a complex network of electrostatic interactions (Figure 1). This finding highlights an innovative role for infigratinib and underscores that, despite being among the most extensively studied enzymes in structural biology[29] kinases continue to reveal unexpected behaviors.

In vitro potency of infigratinib against HCH-associated FGFR3 variants

The inhibitory activity of infigratinib has been assessed against 9 different pathogenic variants associated with HCH (N540K, N540S, N540T, K650Q, K650N, K650T, R223C, T264M, S351F) and was compared with ACH-associated FGFR3 variant (G380R). Mutations across these 9 FGFR3 variants were either in the tyrosine kinase domain (N540K, N540S, N540T, K650Q, K650N, K650T), or in the extracellular domain (R223C, T264M), or in the transmembrane domain (S351F). The in vitro potency (IC50) against each of the 9 variants were in a single digit-nanomolar range with mean IC50 of 3.01 ± 1.81 (mean ± SD) nanomolar (Figure S1). The IC50 of infigratinib against ACH-associated G380R variant was 1.99 ± 0.32 (mean ± SD) nanomolar, suggesting that inhibitory activity of infigratinib against HCH pathogenic variants is very similar to the ACH-associated G380R variant. These data are in line with in silico data showing strong interaction of infigratinib with a HCH-associated variant.

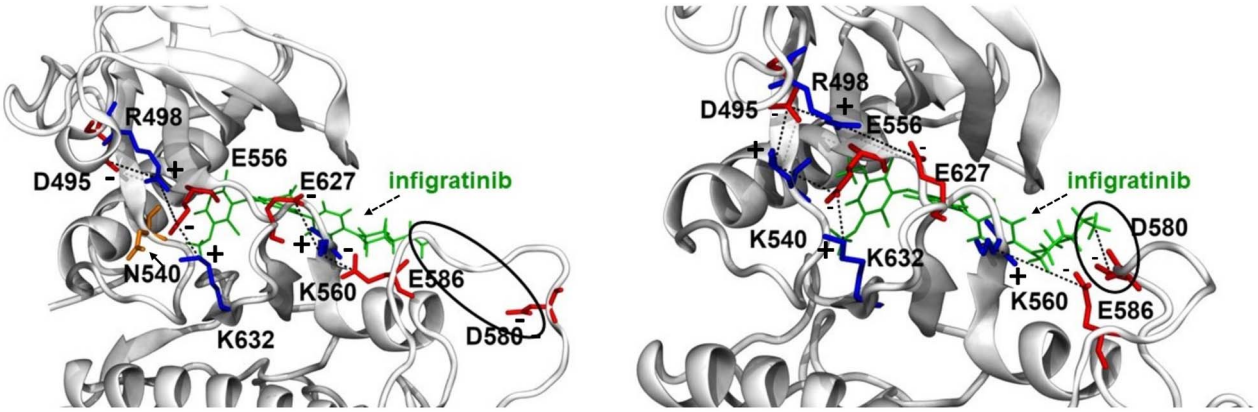

Figure 1. Interaction between infigratinib and the FGFR3 receptor, and the effect of the N540K mutation. Positively charged amino acids (symbol + near negative spot) and negatively charged ones (symbol - near negative spot). Electrostatic favorable interactions are indicated by dashed lines and the neutral residue N540 is shown in plain arrow in the left panel of the figure. In silico modeling shows that infigratinib (dashed arrow) fits similarly in the pocket of the FGFR3 receptor (WT on the left and N540K on the right). The N540K mutation triggers a change in the electrostatic network that moves a loop in one part of the protein, resulting in additional electrostatic interactions (highlighted with an ellipse in the right panel) between infigratinib and D580 in the binding pocket. This favorable interaction is missing in the WT structure (ellipse in the left panel). Abbreviation: FGFR3, FGF receptor 3.

Infigratinib treatment improves skeletal growth in the mouse model of HCH (*Fgfr3*$^{N534K/+}$ mice)

To assess the in vivo efficacy of infigratinib in HCH, we took advantage of the recently developed mouse model of HCH (*Fgfr3*$^{N534K/+}$).[14] Previously, we confirmed that the *Fgfr3*$^{N534K/+}$ mice exhibited a similar skeletal phenotype compared to human pathology, for example, growth deficit with shorter long bones, anomalies of the vertebral body and intervertebral disc (IVD), and domed skull with premature fusion of skull base synchondroses.[14]

Fgfr3$^{N534K/+}$ pup mice were treated with infigratinib according to 2 protocols. Overall, daily administration of 1 mg/kg infigratinib, vehicle treatment, showed statistically significant changes in tail (+4.96% $p < .01$) and L4-L6 (+4.78% $p < .05$) length compared with intermittent dosing (Figure 2, Table 1). At the end of the 21-d period, measurements of the long bones were collected. Compared to vehicle-treated *group*, animals receiving a daily dose of 1 mg/kg infigratinib showed a statistically significant increase in the length of long bones (femur +3.16%, $p < .01$; tibia +3.24%, $p < .01$; humerus +3.03%, $p < .01$; ulna +2.92%,$p < .01$; radius + 3.01% $p < .01$) (Figure 2, Table 1). To assess the effect of the infigratinib treatment on growth, we performed X-rays of the lower limbs clearly showing the growth of the femurs (Figure S2). Skull and mandible shapes are modified in the mouse model of HCH due to abnormalities of mandibular cartilage and skull base synchondroses.[14] Imaging of the skull revealed that after 21 d of infigratinib treatment (daily 1 mg/kg dose) resulted in significant increase in length of the skull (+3.81% $p < .05$) and mandible (+2.52% $p < .01$) compared with the vehicle-treated group (Figure 2). Infigratinib treatment also modified the skull base, as demonstrated by an increase in the dimensions of the foramen magnum length (+3.72% $p < .001$) (Figure 2). All these results confirm the positive impact of infigratinib treatment on both long bone and skull growth.

Next, we compared the magnitude of infigratinib efficacy in the HCH mouse model with that observed in the ACH mouse model.[30] Clinically, skeletal growth deficits associated

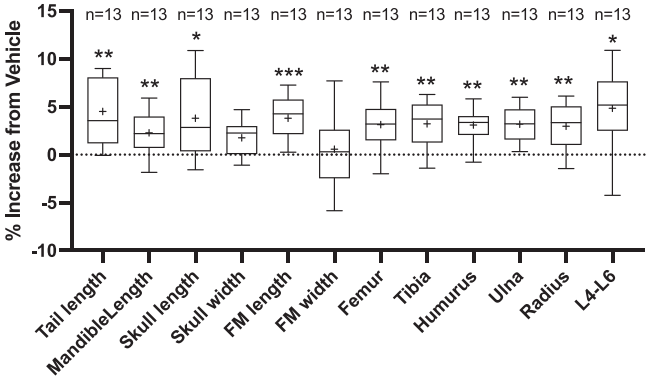

Figure 2. Effects of infigratinib once daily treatment (1 mg/kg) on growth parameters in *Fgfr3*$^{N534K/+}$ mice. Daily dosing: infigratinib 1 mg/kg daily for 21 d (from P3 to P24) in *Fgfr3*$^{N534K/+}$ mice ($n = 13$) . $^{*}p < .05$; $^{**}p < .01$; $^{***}p < .001$ vs vehicle-treated animals.

Table 1. Comparing daily vs intermittent dosing of infigratinib induced changes in skeletal growth parameters in *Fgfr3*$^{N534K/+}$ mice.

	% Change from vehicle	
	Intermittent (1 mg/kg/ every 3 d)	Daily (1 mg/kg/d)
Tail length	+1.20	+4.96**
Mandible length	NA	+2.52**
Skull length	−1.70	+3.81*
Skull width	+0.50	+1.74
Foramen Magnum length	+2.23*	+3.72***
Foramen Magnum width	−2.58	+0.67
Femur	−0.79	+3.16**
Tibia	−0.34	+3.24**
Humerus	+0.10	+3.03**
Ulna	−1.34	+2.92**
Radius	−0.52	+3.01**
L4-L6	+2.65	+4.78*

Intermittent dosing: infigratinib 1 mg/kg every 3 d from P3 to P18 in *Fgfr3*$^{N534K/+}$ mice ($n = 9$); daily dosing: infigratinib 1 mg/kg daily for 21 d (from P3 to P24) in *Fgfr3*$^{N534K/+}$ mice ($n = 13$). NA, data not collected. $^{*}p < .05$. $^{**}p < .01$. $^{***}p < .001$ vs vehicle-treated animals.

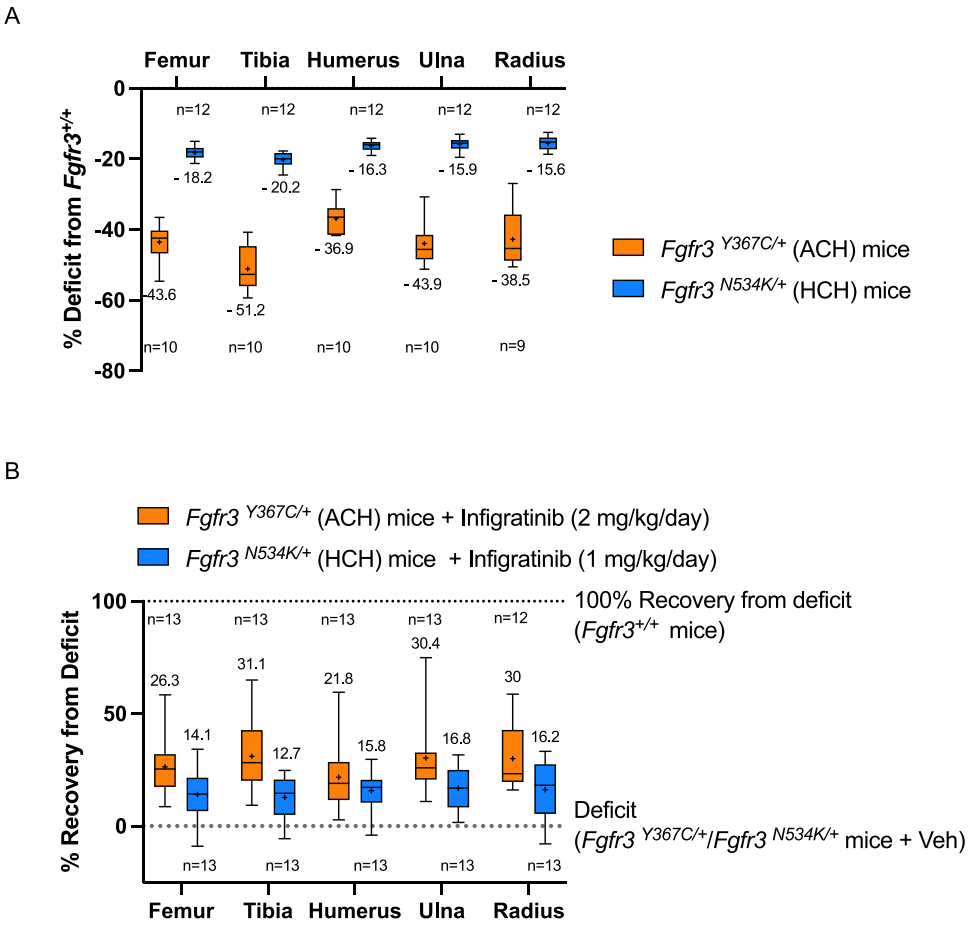

Figure 3. Comparing effects of infigratinib treatment on long bones in HCH (*Fgfr3*$^{N534K/+}$ mice) vs ACH mice (*Fgfr3*$^{Y367C/+}$ mice). (A) Comparing growth deficit of long bones in HCH mice ($n = 12$) and ACH mice ($n = 9$-10) from WT (*Fgfr3* $^{+/+}$ mice). (B) Comparing % recovery from deficit in long bones in response to infigratinib treatment in HCH mice (1 mg/kg/d, $n = 13$) vs ACH mice (2 mg/kg/d, $n = 12$-13). Abbreviations: ACH, achondroplasia, HCH, hypochondroplasia. + sign within box denotes mean value, − sign within box denotes median value, whiskers represent min and max.

with HCH are believed to be less profound than that of ACH.[1] Consistent with the clinical observations, long bone growth deficit in HCH mice compared to WT mice is less profound than in ACH mice (Figure 3A). Due to significant differences in long bone phenotype between HCH and ACH mice, we compared the magnitude of infigratinib efficacy in mouse model of HCH and ACH[30] within the context of their respective growth deficit by assessing the "percent recovery from deficit." As shown in Figure 3B, 1 mg/kg daily treatment of infigratinib in HCH mice resulted in approximately half as much increase in percent recovery from deficit when compared to 2 mg/kg daily treatment of infigratinib in ACH mice. Given that plasma exposures of infigratinib at 1 mg/kg daily dose is half as much as 2 mg/kg daily dose,[31] this suggests that efficacy of infigratinib in improving long bone phenotype is similar in the mouse models of HCH and ACH.

Infigratinib improves growth plate cartilage of long bones and vertebrae in *Fgfr3*$^{N534K/+}$ mice

To evaluate the impact of infigratinib on growth plate cartilage, we analyzed distal and proximal growth plates (data not shown) of the femur in *Fgfr3*$^{N534K/+}$ mice. Daily dosing with infigratinib 1 mg/kg modified the cartilage growth plate in *Fgfr3*$^{N534K/+}$ mice, in particular the distal growth plate cartilage, vs vehicle-treated mice (Figure 4A). Higher magnification of HES staining and Col X labeling highlighted the impact of infigratinib on the shape of hypertrophic chondrocytes. To confirm these immunohistological data, we quantified the hypertrophic area. Infigratinib at the 1 mg/kg dose significantly increased the growth plate hypertrophic area (+20.8% $p < .001$) compared with vehicle treated *Fgfr3*$^{N534K/+}$ mice and significantly reduced the number of hypertrophic chondrocytes (−11.9% $p < .01$) in *Fgfr3*$^{N534K/+}$ mice compared with vehicle treated *Fgfr3*$^{N534K/+}$ mice (Figure 4B and C). Furthermore, infigratinib at the 1 mg/kg dose significantly modified the trabecular bone appearance with Col X immunostaining. The trabecular bone is more abundant in infigratinib-treated *Fgfr3*$^{N534K/+}$ mice compared to vehicle-treated mice confirming the positive impact of the treatment on trabecular bone formation.

MAPK, a canonical signaling pathway downstream of FGFR3, is more active in FGFR3-related disorders.[30] FGF receptor 3 negatively regulates chondrocyte differentiation via the MAPK signaling pathway. Previously, we showed that infigratinib significantly decreases the activation of the MAPK pathway in ACH mouse growth plate cartilage.[31] Here, we performed immunolabeling of phospho-ERK1/2 on growth plate cartilage of distal femur from infigratinib-treated and vehicle treated *Fgfr3*$^{N534K/+}$ mice. Quantification of the phosphorylated ERK1/2 -positive chondrocyte showed a directional reduction in mice treated with infigratinib compared with vehicle treated Fgfr3$^{Y367C/+}$ mice (−25.5% $p = .51$) (Figure 5). These data show that treatment with infigratinib reduced the activity of the MAPK

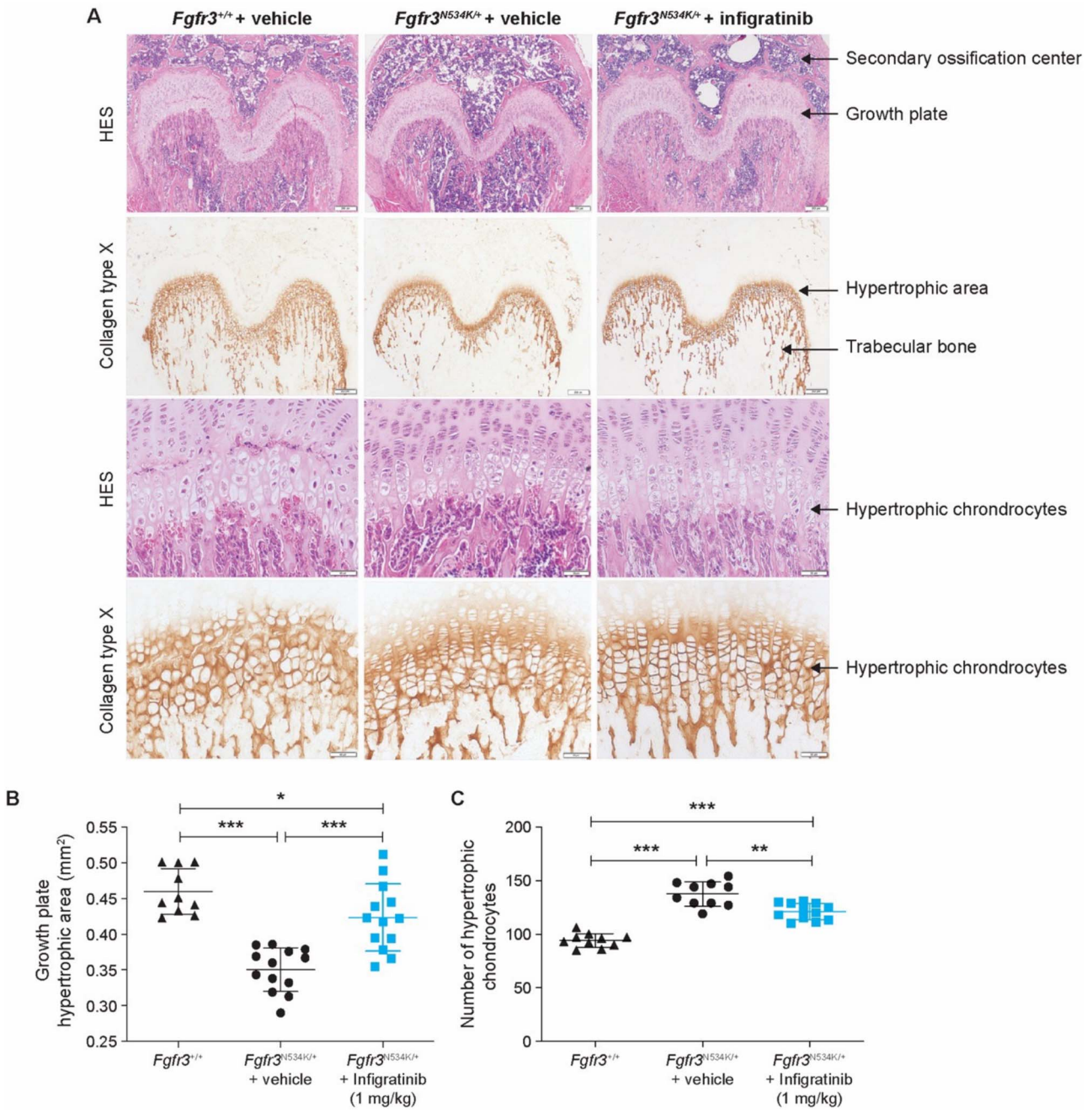

Figure 4. Effect of daily infigratinib on growth plate cartilage. (A) Hypertrophic area of the growth plate in *Fgfr3*$^{+/+}$ *and Fgfr3*$^{N534K/+}$ mice treated with vehicle or daily infigratinib (HES and collagen type X immunolabeling), scale bar (200 μm for top 2 panels, 50 μm for bottom 2 panels). (B) Growth plate hypertrophic area in *Fgfr3*$^{+/+}$ ($n = 10$) and *Fgfr3*$^{N534K/+}$ mice ($n = 13$) treated with vehicle and *Fgfr3*$^{N534K/+}$ mice ($n = 13$) treated with infigratinib. (C) Number of hypertrophic chondrocytes in the distal femur of *Fgfr3*$^{+/+}$ ($n = 10$) and *Fgfr3*$^{N534K/+}$ mice ($n = 12$) treated with vehicle and *Fgfr3*$^{N534K/+}$ mice ($n = 10$) treated with infigratinib. $^{*}p < .05$; $^{**}p < .01$; $^{***}p < .001$. Abbreviation: HES, H&E staining.

pathway thus suggesting that phosphorylation of FGFR3 is decreased.

To complete this growth plate cartilage analysis, we investigated whether infigratinib treatment also altered vertebral cartilage endplate and IVD area (Figure 6A) and bone part of the vertebra (Figure 6B). Histological and immunohistological analyses were performed to assess the extent of lumbar vertebral and IVD changes due to infigratinib treatment. The study of the cartilage endplate organization of the vertebrae using HES staining and Col X immunolabeling show that the hypertrophic growth plate area of the cartilage endplate was significantly increased with infigratinib treatment (superior area + 32.4% $p < .001$ and inferior area + 30.8% $p < .001$), and in the same way IVD area was significantly increased (+10.6% $p < .05$) (Figure 6A). Studying the L5 trabecular bone, we observed an increase in the surface area of the bony part (+10.1% $p < .001$) (Figure 6B).

Overall data from treatment with infigratinib on cartilage growth plate and endplate show a positive effect on both axial and appendicular skeleton.

Discussion

Similar to ACH, the underlying cause of HCH is overactivity of FGFR3 signaling due to gain-of-function mutations in FGFR3. While ACH is mainly caused by transmembrane

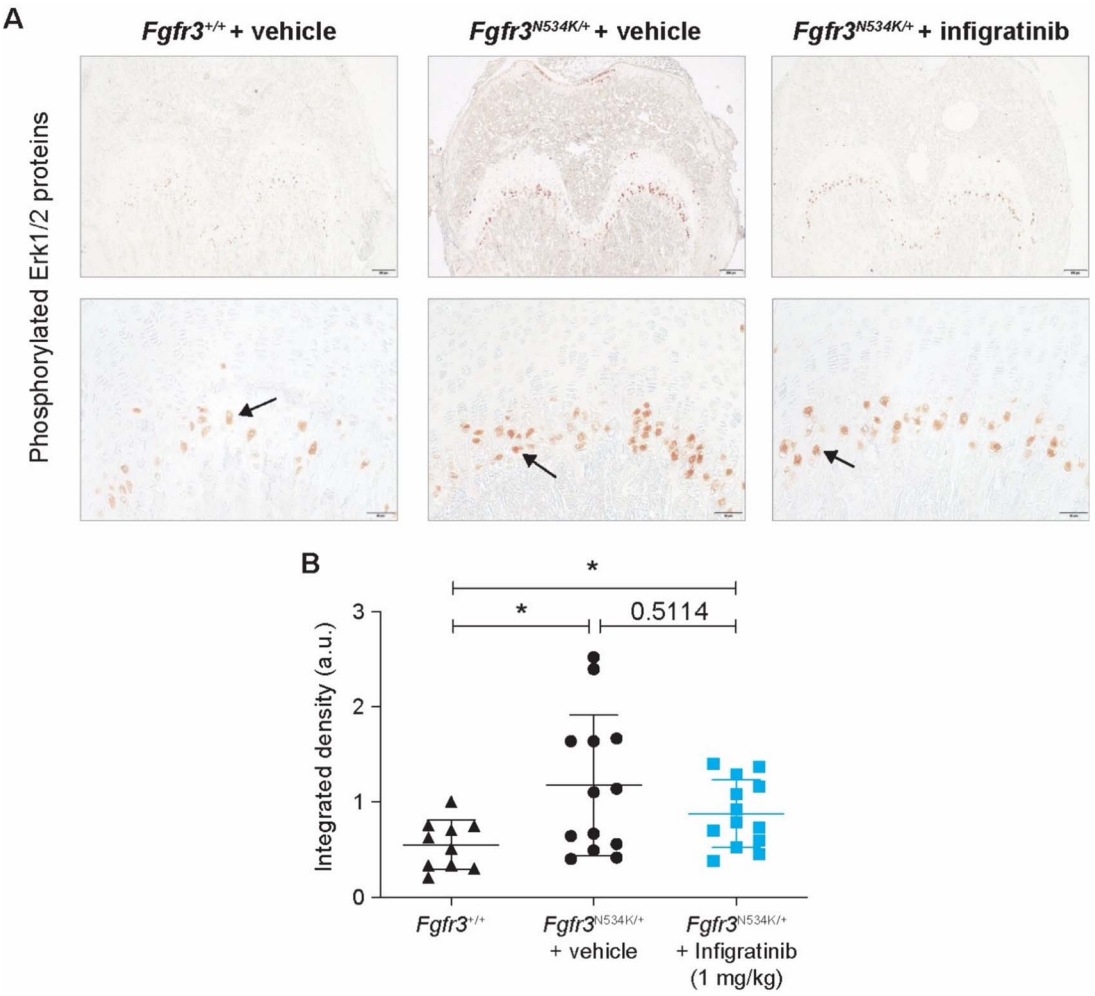

Figure 5. Effect of daily infigratinib on MAPK signaling. (A) Representative images of phospho-ERK1/2 immunostaining in the growth plate cartilage of distal femurs in *Fgfr3*$^{+/+}$ *and Fgfr3*$^{N534K/+}$ mice treated with vehicle or daily infigratinib. Arrows indicate positive cells (scale bar 200 μm for top panel; scale bar 50 μm for bottom panel). (B) Infigratinib treatment (1 mg/kg/d) induced reduction in phosphorylation of ERK1/2 proteins in the *Fgfr3*$^{N534K/+}$ cartilage growth plate ($n = 13$) vs the vehicle treated *Fgfr3*$^{N534K/+}$ growth plate ($n = 13$), similar to phosphorylation levels in the *Fgfr3*$^{+/+}$ growth plate ($n = 11$). a.u., arbitrary units; $*p < .05$.

domain localized mutation G380R, HCH is driven by different gain-of-function mutations localized in different domains such as the tyrosine kinase domain. Given that infigratinib treatment has demonstrated robust efficacy in ACH mice,[30,31] and has yielded promising efficacy data in a phase 2 trial of children with ACH,[15] we hypothesized that infigratinib is a viable therapeutic strategy for the treatment of HCH via countering FGFR3 overactivity. In this study, we tested therapeutic impact of infigratinib on HCH by conducting in silico, in vitro and in vivo studies.

In silico analysis with WT FGFR3 and N540K FGFR3 variant demonstrated that infigratinib interacts with both the WT and mutated FGFR3 complexes, with a stronger interaction observed in the presence of the N540K mutation. In vitro studies with 9 different HCH-associated pathogenic FGFR3 variants have demonstrated that infigratinib has single digit-nanomolar potency and is comparable with the ACH-associated FGFR3 variant (G380R). These data suggest that infigratinib has the potential to counteract the underlying FGFR3 overactivity in HCH. In vivo data in HCH mice demonstrates that 1 mg/kg dose of infigratinib ameliorated the clinical hallmarks of human pathology and significantly increased the length of the axial skeleton, the appendicular skeleton, and improved foramen magnum length. Results were significantly better with daily vs intermittent dosing across all parameters investigated. Although infigratinib treatment resulted in a significant increase in long bone lengths in HCH mice, the magnitude of this increase appears to be smaller in HCH mice when compared to ACH mice.[30] We hypothesized that this could be explained by HCH mice having a milder long bone phenotype (lesser deficit from WT mice) compared to ACH mice (higher deficit from WT mice). To better contextualize this difference, we investigated if efficacy differences can be explained by severity of growth deficit of HCH and ACH mice compared to WT mice. By comparing infigratinib efficacy in HCH mice and ACH mice by assessing "percent recovery from deficit," we find that infigratinib efficacy in HCH is similar to ACH mice, which is consistent with comparable in vitro potency at ACH and HCH-associated FGFR3 variants. It is important to point out 2 key differences in infigratinib treatment in HCH and ACH mice. In HCH mice, infigratinib dosing was initiated on P3 and treatment duration was 3 wk. In ACH mice, infigratinib dosing was initiated on P1 and treatment duration was 2 wk.[30] Recent work from Rico-Llanos and colleagues[32] suggest that long bone growth in response to infigratinib is similar despite varied treatment

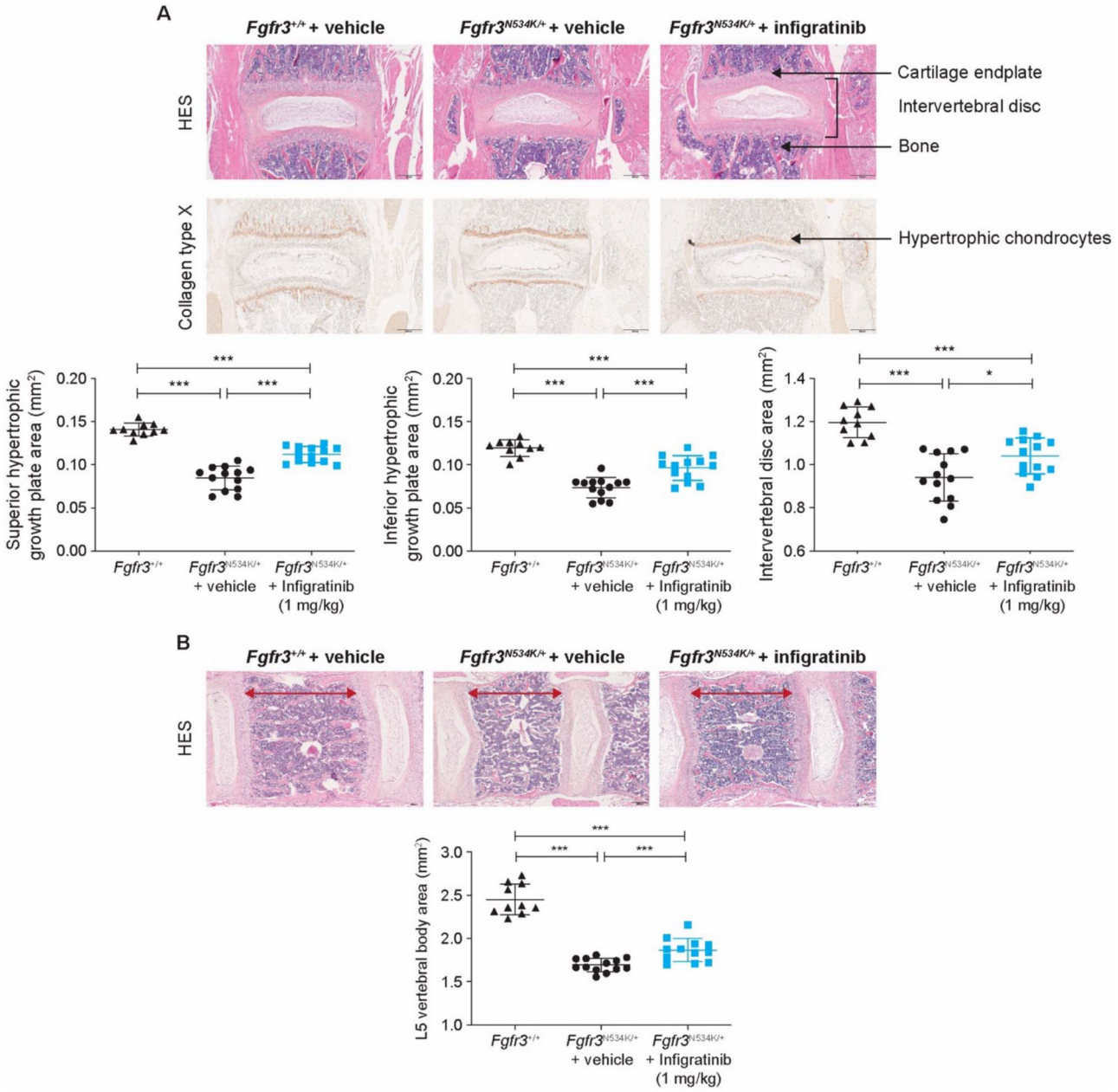

Figure 6. Effect of daily infigratinib on axial skeletal. (A) Representative histological picture of HES staining and collagen type X immunolabeling of the intervertebral disc in *Fgfr3*$^{+/+}$ *and Fgfr3*$^{N534K/+}$ mice treated with vehicle or daily infigratinib (scale bar 200 μm). Infigratinib treatment induced a significant increase of hypertrophic growth plate areas of the cartilage endplate, and intervertebral disc area in *Fgfr3*$^{N534K/+}$ mice ($n = 13$) compared to vehicle treated *Fgfr3*$^{N534K/+}$ mice ($n = 13$). (B) Representative histological picture of HES of L5 vertebral body area (scale bar 200 μm). Infigratinib treatment induced a significant improvement in lumbar vertebrae bone area in *Fgfr3*$^{N534K/+}$ mice ($n = 13$) compared to vehicle treated *Fgfr3*$^{N534K/+}$ mice ($n = 13$) ($^{*}p < .05$; $^{**}p < .01$; $^{***}p < .001$). Abbreviation: HES, H&E staining.

initiation time and duration, suggesting that comparison of infigratinib effect on long bone growth in ACH and HCH mice is relevant despite differences in treatment initiation and duration. For the in vivo studies in mice, despite having oral bioavailability, infigratinib was dosed via sub cutaneous route as oral gavage is not feasible at P3.

In addition, improvements in cartilage growth plate and bone parameters were also observed in *Fgfr3*$^{N534K/+}$ mice treated with daily infigratinib, with increased hypertrophic area and reduced number of hypertrophic chondrocytes, and increased bone formation compared with vehicle. Downstream effects on the MAPK pathway (ERK1/2 phosphorylation) controlling chondrocyte differentiation was also observed in infigratinib-treated *Fgfr3*$^{N534K/+}$ mice. These findings are in line with results from the ACH mouse model, indicating infigratinib treatment reduces the overactivity of FGFR3 and downstream signaling.[30]

Clinical trials evaluating infigratinib in children with ACH are currently underway, with promising initial results. In a phase 2 clinical study in children with ACH, oral administration of infigratinib at a dose of 0.25 mg/kg/d resulted in a statistically significant increase in AHV, which persisted throughout the duration of the study, with 2.5 cm/yr in mean change from baseline at 18 mo.[15] Notably, treatment with the study drug at the dose of 0.25 mg/kg/d resulted in a persistent and statistically significant decrease in the upper/lower body segment ratio suggesting a potential improvement in body proportions. Treatment with infigratinib at the doses explored

and for the duration evaluated was considered generally safe and well tolerated. Furthermore, increase in AHV was supported by a concomitant increase in collagen X biomarker. The efficacy and safety of infigratinib in children with ACH is currently being investigated in the double blind, placebo-controlled phase 3 study (NCT06164951). In conclusion, daily infigratinib 1 mg/kg administered to the *Fgfr3*$^{N534K/+}$ mouse counteracted the constitutive activation of FGFR3 resulting from the heterozygous N540K pathogenic variant localized in the kinase domain of *FGFR3*. These results provide a strong biological and pharmacological rationale for targeting FGFR3 with infigratinib for the treatment of children with HCH.

Acknowledgments

We thank Emilie Panafieu from LEAT-Imagine Institute-SFR Necker for her help for this work. We would also like to thank the Philanthropy Department of Mutuelles AXA through the "Head and Heart Chair" for supporting the Imagine Institute's imaging facility.

Author contributions

Benoit Demuynck (Formal analysis, Methodology, Validation), Bhavik Shah (Resources, Writing—original draft, Writing—review & editing), Franck Mayeux (Validation, Writing—original draft), Laurine Vasseur (Software), Florent Barbault (Conceptualization, Methodology, Writing—original draft), Jixin Ding (Writing—original draft), Morgan Paull (Funding acquisition, Writing—review & editing), Tejaswini Reddi (Writing—original draft), Elena Muslimova (Validation, Writing—review & editing), and Laurence Legeai-Mallet (Conceptualization, Funding acquisition, Supervision, Writing—original draft, Writing—review & editing)

B.D. and B.P.S. contributed equally to the work and should be considered co-first authors.

Supplementary material

Supplementary material is available at *Journal of Bone and Mineral Research* online.

Funding

This work was supported in part by a grant from BridgeBio/QED Therapeutics. This project received a state subsidy managed by Research fund AXA and the Philanthropy Department of Mutuelles AXA through the Head and Heart chair. The authors also thank ANR PIRATE for their financial support and GENCI computing centers and the Platform P3MB for computational resources.

Conflicts of interest

B.P.S., J.D., M.P., T.R., and E.M. are employees and shareholders of BridgeBio Pharma. B.D., F.M., L.V., F.B., and L.L.M. have declared no competing interests.

Data availability

The data that support the findings of this study are available from the corresponding author.

References

1. Bober MB, Bellus GA, Nikkel SM, et al. Hypochondroplasia. 1999 Jul 15 [updated 2020 may 7]. In: Adam MP, Feldman J, Mirzaa GM, et al., eds. *GeneReviews*. University of Washington, Seattle; 1993-2025: https://www.ncbi.nlm.nih.gov/books/NBK1477/
2. Sabir AH, Sheikh J, Singh A, et al. Earlier detection of hypochondroplasia: a large single-center UK case series and systematic review. *Am J Med Genet A*. 2021;185(1):73-82.
3. Linnankivi T, Mäkitie O, Valanne L, et al. Neuroimaging and neurological findings in patients with hypochondroplasia and FGFR3 N540K mutation. *Am J Med Genet A*. 2012;158a(12):3119-3125.
4. Ahmadi M, Herting A, Mueffelmann B, et al. Hypochondroplasia and temporal lobe epilepsy – a series of 4 cases. *Epilepsy Behav*. 2022;126:108479.
5. Okazaki T, Saito Y, Ueda R, et al. Epileptic phenotype of FGFR3-related bilateral medial temporal lobe dysgenesis. *Brain Dev*. 2017;39(1):67-71.
6. Rangos N, Dwivedi P, Boucher K, et al. Parent-reported quality of life of children with hypochondroplasia: baseline results from a clinical trial. *Horm Res Paediatr*. 2023;96(Suppl 3):195-196.
7. Arenas MA, Del Pino M, Fano V. FGFR3-related hypochondroplasia: longitudinal growth in 57 children with the p.Asn540Lys mutation. *J Pediatr Endocrinol Metab*. 2018;31(11):1279-1284.
8. Cheung MS, Cole TJ, Arundel P, et al. Growth reference charts for children with hypochondroplasia. *Am J Med Genet A*. 2024;194(2):243-252.
9. Bellus GA, McIntosh I, Smith EA, et al. A recurrent mutation in the tyrosine kinase domain of fibroblast growth factor receptor 3 causes hypochondroplasia. *Nat Genet*. 1995;10(3):357-359.
10. Le Merrer M, Rousseau F, Legeai-Mallet L, et al. A gene for achondroplasia-hypochondroplasia maps to chromosome 4p. *Nat Genet*. 1994;6(3):318-321.
11. Lemmon MA, Schlessinger J. Cell signaling by receptor tyrosine kinases. *Cell*. 2010;141(7):1117-1134.
12. Rousseau F, Bonaventure J, Legeai-Mallet L, et al. Mutations in the gene encoding fibroblast growth factor receptor-3 in achondroplasia. *Nature*. 1994;371(6494):252-254.
13. Heuertz S, Le Merrer M, Zabel B, et al. Novel FGFR3 mutations creating cysteine residues in the extracellular domain of the receptor cause achondroplasia or severe forms of hypochondroplasia. *Eur J Hum Genet*. 2006;14(12):1240-1247.
14. Loisay L, Komla-Ebri D, Morice A, et al. Hypochondroplasia gain-of-function mutation in FGFR3 causes defective bone mineralization in mice. *JCI Insight*. 2023;8(12):e168796.
15. Savarirayan R, Bergua JMD, Arundel P, et al. Oral infigratinib therapy in children with achondroplasia [published online November 18, 2024. *N Engl J Med*. 2025;392(9):865-874. https://doi.org/10.1056/NEJMoa2411790
16. Kuriwaki I, Kameda M, Iikubo K, et al. Synthesis and structure-activity relationships of pyrimidine derivatives as potent and orally active FGFR3 inhibitors with both increased systemic exposure and enhanced in vitro potency. *Bioorg Med Chem*. 2021;33:116019.
17. Jonquoy A, Mugniery E, Benoist-Lasselin C, et al. A novel tyrosine kinase inhibitor restores chondrocyte differentiation and promotes bone growth in a gain-of-function Fgfr3 mouse model. *Hum Mol Genet*. 2012;21(4):841-851.
18. Li Y, Delamar M, Busca P, et al. Molecular modeling study of the induced-fit effect on kinase inhibition: the case of fibroblast growth factor receptor 3 (FGFR3). *J Comput Aided Mol Des*. 2015;29(7):619-641.
19. Case D, Aktulga HM, Belfon K, et al. *Amber 2023*. University of California; 2023.
20. Humphrey W, Dalke A, Schulten K. VMD: visual molecular dynamics. *J Mol Graph*. 1996;14(1):33-38.
21. Roe DR, Cheatham TE 3rd. PTRAJ and CPPTRAJ: software for processing and analysis of molecular dynamics trajectory data. *J Chem Theory Comput*. 2013;9(7):3084-3095.
22. Torrie GM, Valleau JP. Nonphysical sampling distributions in Monte Carlo free-energy estimation: umbrella sampling. *J Comput Phys*. 1977;23(2):187-199.
23. Grossfield A. WHAM: the weighted histogram analysis method. version XXXX; http://membrane.urmc.rochester.edu/wordpress/?page_id=126
24. Yao Y, Wang Y. ATDC5: an excellent in vitro model cell line for skeletal development. *J Cell Biochem*. 2013;114(6):1223-1229.

25. Attwood MM, Fabbro D, Sokolov AV, et al. Trends in kinase drug discovery: targets, indications and inhibitor design. *Nat Rev Drug Discov*. 2021;20(11):839-861.
26. Modi V, Dunbrack RL Jr. Defining a new nomenclature for the structures of active and inactive kinases. *Proc Natl Acad Sci USA*. 2019;116(14):6818-6827.
27. Cohen P, Cross D, Jänne PA. Kinase drug discovery 20 years after imatinib: progress and future directions. *Nat Rev Drug Discov*. 2021;20(7):551-569.
28. Möbitz H. The ABC of protein kinase conformations. *Biochim Biophys Acta*. 2015;1854(10 Pt B):1555-1566.
29. Ferguson FM, Gray NS. Kinase inhibitors: the road ahead. *Nat Rev Drug Discov*. 2018;17(5):353-377.
30. Komla-Ebri D, Dambroise E, Kramer I, et al. Tyrosine kinase inhibitor NVP-BGJ398 functionally improves FGFR3-related dwarfism in mouse model. *J Clin Invest*. 2016;126(5):1871-1884.
31. Demuynck B, Flipo J, Kaci N, et al. Low-dose infigratinib increases bone growth and corrects growth plate abnormalities in an achondroplasia mouse model. *J Bone Miner Res*. 2024;39(6):765-774.
32. Rico-Llanos G, Spoutil F, Blahova E, et al. Achondroplasia: aligning mouse model with human clinical studies shows crucial importance of immediate postnatal start of the therapy. *J Bone Miner Res*. 2024;39(12):1783-1792.

Journal of Bone and Mineral Research, 2025, 00, 1–10
https://doi.org/10.1093/jbmr/zjaf088
Research Article